High-temperature phase transitions of hexagonal $YMnO_3$

Alexandra S. Gibbs,[1,2] Kevin S. Knight,[3] and Philip Lightfoot[1,*]

[1]*School of Chemistry and EaStCHEM, University of St Andrews, North Haugh, St Andrews KY16 9ST, United Kingdom*

[2]*Scottish Universities Physics Alliance (SUPA), School of Physics and Astronomy, University of St Andrews, North Haugh, St Andrews KY16 9SS, United Kingdom*

[3]*ISIS Facility, Rutherford Appleton Laboratory, Chilton, Didcot OX11 OQX, United Kingdom*

(Received 13 August 2010; revised manuscript received 18 November 2010; published 8 March 2011)

We report a detailed high-resolution powder neutron diffraction investigation of the structural behavior of the multiferroic hexagonal polymorph of $YMnO_3$ between room temperature and 1403 K. The study was aimed at resolving previous uncertainties regarding the nature of the paraelectric-ferroelectric transition and the possibilities of any secondary structural transitions. We observe a clear transition at 1258 ± 14 K corresponding to a unit-cell tripling and a change in space group from centrosymmetric $P6_3/mmc$ to polar $P6_3cm$. Despite the fact that this symmetry permits ferroelectricity, our experimental data for this transition (analyzed in terms of symmetry-adapted displacement modes) clearly support previous theoretical analysis that the transition is driven primarily by the antiferrodistortive K_3 mode. We therefore verify previous suggestions that $YMnO_3$ is an improper ferrielectric. Furthermore, our data confirm that the previously suggested intermediate phase with space group $P6_3/mcm$ does not occur. However, we do find evidence for an isosymmetric phase transition (i.e., $P6_3cm$ to $P6_3cm$) at ≈920 K, which involves a sharp decrease in polarization. This secondary transition correlates well with several previous reports of anomalies in physical properties in this temperature region and may be related to Y-O hybridization.

DOI: 10.1103/PhysRevB.83.094111 PACS number(s): 61.05.fm, 61.50.Ks, 77.80.−e

I. INTRODUCTION

The $AMnO_3$ manganites (with $A =$ Lanthanide, In, Y, and Sc) have attracted much interest in recent years due to their multiferroic properties.[1,2] Two structural forms of these materials exist, both displaying multiferroicity.[3] The orthorhombic form, a perovskite with room-temperature space group *Pnma*, occurs for $A =$ La-Tb. The hexagonal form (with a layered structure) shown in Fig. 1(a) is favored for $A =$ Dy-Lu, In, Y, and Sc. Varying the synthesis technique, however, allows for some flexibility of this trend.[3] The space group of the hexagonal polymorph at room temperature, as determined by Yakel *et al.* in 1963,[4] is $P6_3cm$.

$YMnO_3$ can be synthesized in either of the two polymorphs. The hexagonal form is obtained when standard ambient-pressure solid-state synthesis conditions are used. This form has Mn^{3+} ions coordinated by five oxide ions, forming a trigonal bipyramid. The Y^{3+} ions are coordinated by eight oxide ions (six equatorial oxygens from two symmetry inequivalent sites and two inequivalent apical oxygens). The bipyramids are tilted with respect to the *c*-axis, and the two Y–O apical bond lengths for each yttrium site are unequal as a result of this.

The hexagonal manganites are ferrielectric[5] (the term here referring to the dipole moments due to the two symmetry inequivalent Y^{3+} sites, which are aligned in an antiparallel manner but are of unequal magnitude, leading to a net polarization) up to high temperatures in excess of $T_C \approx$ 900 K (Refs. 6 and 7) and order antiferromagnetically below $T_N \approx 70$ K.[8,9] The ferrielectricity is due to opposing dipoles caused by opposite but unequal displacements of the two yttrium sites and the associated tilting and distortion of the MnO_5 bipyramids.[10,11] This is an unusual driving mechanism for ferroelectricity and has been termed geometric ferroelectricity,[11] as it seems to depend purely on ionic size effects rather than on the more ubiquitous electronic effects such as d^0 cation Jahn-Teller distortions (Ti^{4+}, Nb^{5+}, etc.)[12] or the presence of stereochemically active s^2 lone pair cations such as Pb^{2+} or Bi^{3+}.

Due to the experimental difficulties in measuring physical properties such as the dielectric constant at the high temperatures of the ferrielectric phase transition, ambiguity exists about the mechanism and exact nature of the transition between the polar $P6_3cm$ structure and the centrosymmetric $P6_3/mmc$ state [shown in Fig. 1(b)], which is suggested to exist above ≈1250 K. This aristotype structure is the undistorted form of the ambient-temperature structure. The low-temperature structure is generated from the aristotype by loss of mirror symmetry perpendicular to the *c*-axis, resulting in tilted MnO_5 bipyramids, unequal apical Y–O bond lengths, and a larger unit cell, with three times the $P6_3/mmc$ unit-cell volume and the low-temperature unit-cell parameters $a = \sqrt{3}a'$, $c = c'$.

Previous studies have produced a wide range of transition temperatures using various methods, tabulated in Table I, for both the ferrielectric transition temperature (T_C) and the unit-cell tripling transition between $P6_3/mmc$ and $P6_3cm$ (T_S), which tilts the MnO_5 trigonal bipyramids (untilted in the high-temperature $P6_3/mmc$ phase) and corrugates the Y^{3+} layers leading to tripling of the *ab*-plane unit-cell area and, therefore, the unit-cell volume.

The variety of transition temperatures measured has been attributed to impurities introduced by the synthesis method,[18] but the subtle nature of the transitions and lack of polarization or thermodynamic measurements also make transition temperatures difficult to define.

The possibility of an intermediate phase between $P6_3/mmc$ and $P6_3cm$ has been noted.[17,21,22] The possible intermediate phases were identified using group theoretical arguments;[10,21] a diagram of the possible transition paths is shown in Fig. 2.

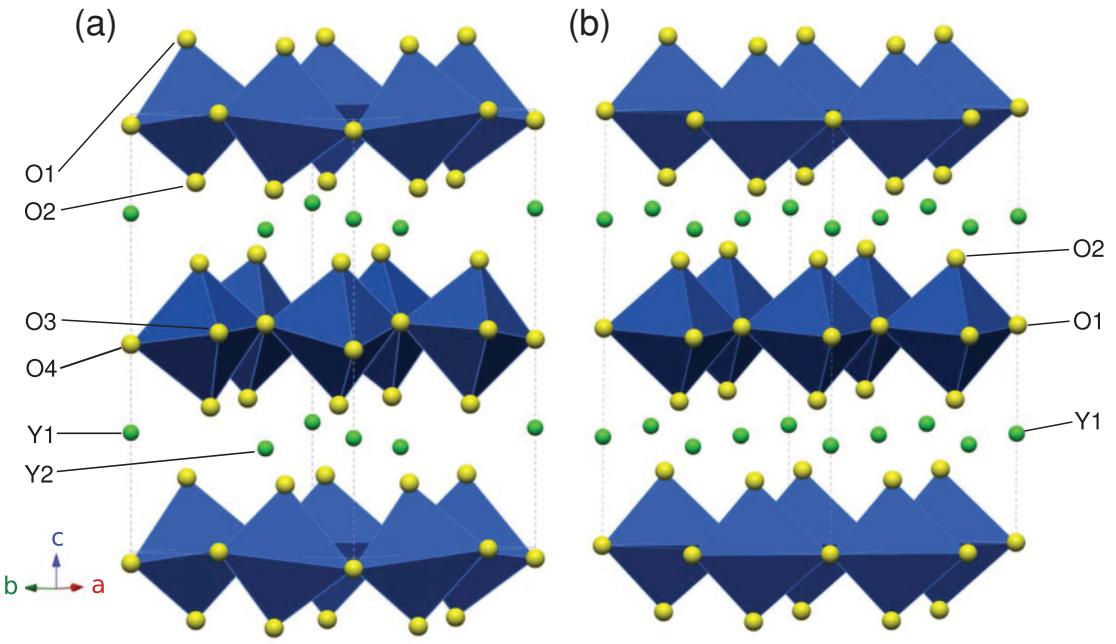

FIG. 1. (Color online) (a) The ambient-temperature polar $P6_3cm$ structure of hexagonal $YMnO_3$. (b) The high-temperature centrosymmetric $P6_3/mmc$ form displayed in the $P6_3cm$ basis to allow comparison (transformation matrix: $[a+b, -a+2b, c+\frac{1}{4}]$). The Y atoms (green) are eightfold coordinated by oxygen (yellow) and the Mn atoms are fivefold coordinated (blue polyhedra).

The transition from $P6_3/mmc$ to $P6_3/mcm$ would involve unit-cell tripling caused by displacement of the O1-Mn-O1 axis within the *ab* plane, but no tilt of the MnO_5 bipyramids or Y^{3+} displacement. Taking the path from $P6_3/mmc$ to $P6_3mc$ would involve no change in unit-cell volume, only loss of the mirror plane allowing independent polar displacements of all atoms along *c*. Therefore, the most straightforward method of identifying the transition path is to determine whether the cell tripling occurs at the same point as the polar displacement and to examine the Y site splitting and tilt of the MnO_5 bipyramids.

TABLE I. The previously reported transition temperatures of the ferrielectric (T_C) and unit-cell tripling (T_S) transitions. PXRD = powder x-ray diffraction, SXD = single-crystal x-ray diffraction, PND = powder neutron diffraction, DTC = differential thermal calorimetry, and MEM = maximum entropy method.

Reference	T_C (K)	T_S (K)	Method
Coeuré *et al.*[6]	913		Dielectric permittivity
Ismailzade and Kizhaev[13]	933		Pyroelectric current and SXD
Łukaszewicz and Karat-Kalicińska[14]		1275	SXD
Katsufuji *et al.* (2001)[15]	910		Resistivity
Katsufuji *et al.* (2002)[16]	$\geqslant$1000	$\geqslant$1000	PXRD
Nénert *et al.* (2005)[17]	1020	1273	SXD
Nénert *et al.* (2007)[18]	1125	1350	Powder DTC
Jeong *et al.*[19]		$\geqslant$1200	PND
Choi *et al.*[2]	$\approx$880		Resistivity
Kim *et al.*[20]	$\approx$920		PXRD (MEM)

Although Nénert *et al.*[18] proposed $P6_3/mcm$ as the intermediate phase, no structural parameters from their intermediate phase region were published. Therefore, a systematic variable temperature study with careful examination of the distortions of the structure and comparative refinements of alternative space groups is required.

Most crystallographic studies thus far have used powder x-ray diffraction, which usually does not allow such reliable and precise determination of lattice parameters and atomic positions in oxide materials as neutron diffraction. This therefore increases the difficulty of pinning down the location and nature of the phase transitions. The only previous powder-neutron study[19] involved four temperatures between 1000 and 1400 K and left the key issues unresolved. To

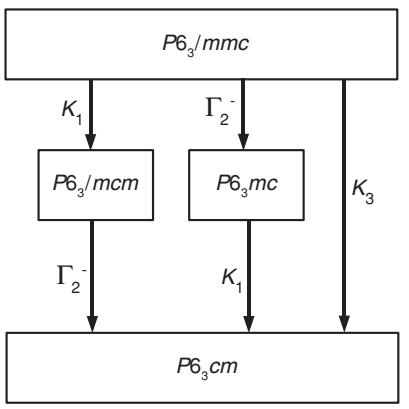

FIG. 2. The group-subgroup relation diagram for the transition between centrosymmetric $P6_3/mmc$ and polar $P6_3cm$. The arrow labels denote the distortion modes leading to the lower symmetry space groups, and the *K* modes are unit-cell tripling modes.

attempt to resolve this uncertainty, we have undertaken a higher-resolution powder-neutron-diffraction study using finer temperature intervals.

II. EXPERIMENT

A. Sample synthesis and characterization

A single-phase polycrystalline sample was prepared by standard solid-state synthesis. A stoichiometric mixture of Y_2O_3 (Sigma Aldrich 99.999%) and MnO_2 (Sigma Aldrich 99.99+%) was ground under acetone, pressed into pellets, and heated at 1473 K on sacrificial powder in an alumina boat for 140 hours with intermediate grindings every 18 hours. The sample quality was monitored using laboratory x-ray diffraction (Stoe STADI P with Cu $K_{\alpha 1}$ source in flat-plate transmission mode) throughout the synthesis to ensure that a phase-pure sample was obtained. Energy dispersive x-ray (EDX) spectroscopy was also used to confirm that the sample was not contaminated by, for example, aluminium from the alumina crucible.

B. Powder neutron diffraction

Powder neutron diffraction was undertaken on the high-resolution powder diffractometer (HRPD) at ISIS.[23,24] A 5-g sample was sealed in a quartz tube and placed in a cylindrical vanadium can mounted in a standard furnace. Data were collected at 28 temperatures between 293 and 1403 K (every 60 K from 373 to 1093 K and then at intervals of 10–30 to 1403 K) with appropriate equilibration times at each temperature before commencement of data collection. The data used for the analysis were all taken from the backscattering detector bank centered at 168° with resolution $\frac{\Delta d}{d} \approx 4 - 5 \times 10^{-4}$. Data were refined using the Rietveld method with the program GSAS.[25] A 20-term shifted Chebyshev background function was used to account for the substantial quartz background, and appropriate absorption corrections were applied. Small peaks from the vanadium can were identified in all patterns, and these were not included in the refinements.

III. RESULTS

A. High-temperature phase

The transition from the high-temperature $P6_3/mmc$ phase to the low-temperature unit-cell tripled phase is signaled most clearly by the appearance of the (202) peak due to the factor of $\sqrt{3}$ increase in a as shown in Fig. 3. Another section of the diffraction pattern showing the appearance of two further peaks is included in the supplemental information.[27] The (202) peak is absent in all datasets above the 1243-K dataset where it first appears. It then increases in intensity with decreasing temperature. The diffraction patterns have no reflections breaking $P6_3/mmc$ symmetry at 1273 K or above. The Rietveld refinements in the high-temperature phase converged quickly, and anisotropic thermal displacement factors were refined for all sites. Refined structural parameters in the $P6_3/mmc$ phase at 1303 K are given in Table II.

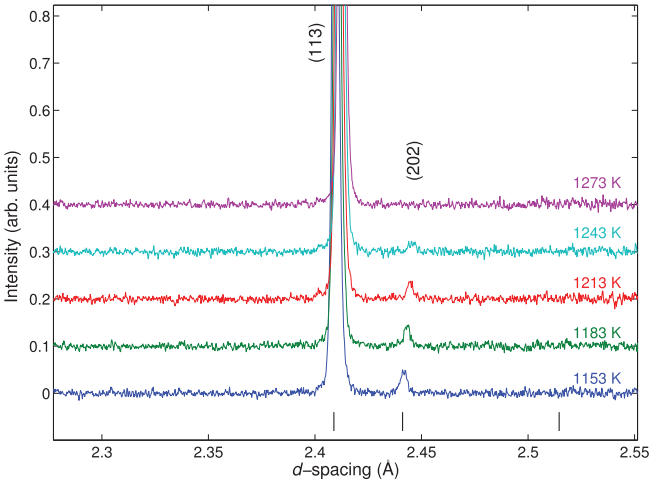

FIG. 3. (Color online) A portion of the raw diffraction patterns for 1153, 1183, 1213, 1243, and 1273 K offset by 0.1 on the intensity axis for clarity. The appearance of the (202) peak at 2.44 Å signals the entry into the polar $P6_3cm$ phase.

The smooth variation of the thermal displacement factors[27] and lattice parameters with temperature in this high-temperature regime suggest that there is no higher temperature phase transition. Refinements in the polar space group $P6_3mc$ in the same unit cell did not give improved fits.[27] Moreover, there is no previous evidence of any physical property measurements supporting the occurrence of a noncentrosymmetric phase at this temperature. There is also no indication, within the temperature range studied, of a transition to a further high-temperature polymorph in space group $P6/mmm$, which was recently proposed by Abrahams[22] to be the aristotype structure present above the $P6_3/mmc$ phase. This structure, predicted to occur above $\gtrsim$1600 K, would have a halved c-axis

TABLE II. The structural parameters for the 1303-K data refined in $P6_3/mmc$ (No. 194). The lattice parameters are $a = 3.618\,961(15)$ Å and $c = 11.340\,90(9)$ Å.[a] The refinement gave $wR_p = 0.0331$, $\chi^2 = 6.356$.

Atom	Wyckoff position	x	y	z	$u_{11}/u_{22} \times 100$ (Å^2)	$u_{33} \times 100$ (Å^2)	$u_{12} \times 100$ (Å^2)
Y1	$2a$	0	0	0	2.01(3)	6.75(5)	1.004(16)
Mn	$2c$	$\frac{1}{3}$	$\frac{2}{3}$	$\frac{1}{4}$	3.97(5)	1.61(7)	1.99(2)
O1	$2b$	0	0	$\frac{1}{4}$	3.35(4)	6.64(8)	1.69(2)
O2	$4f$	$\frac{1}{3}$	$\frac{2}{3}$	0.085 57(7)	3.52(3)	1.84(4)	1.760(16)

[a]The uncertainties in the lattice parameters obtained from GSAS have been multiplied by a factor of 3 to comply with the request of an anonymous referee (Ref. 26).

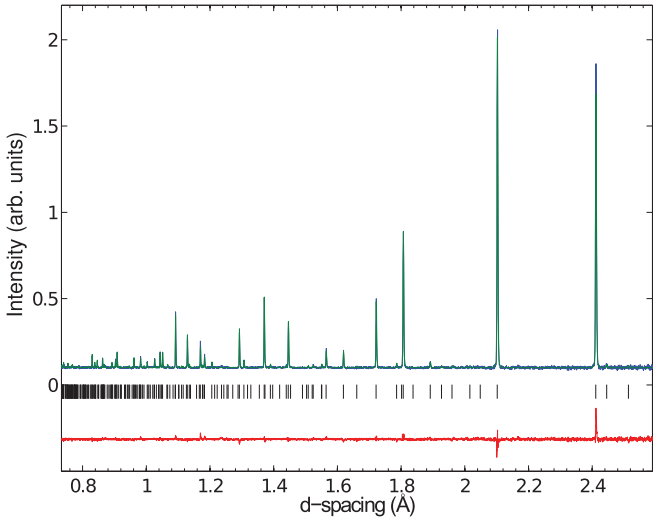

FIG. 4. (Color online) The full-range fit resulting from the Rietveld refinement of the 1243-K dataset with the $P6_3cm$ model. The blue line is the raw data, the green line is the Rietveld fit, the red line is the difference profile, and the black markers indicate predicted reflection positions.

length relative to the other phases and would require a large displacement (≈0.99 Å) in oxide ion positions. It should be noted, however, that the highest temperature data in this study was taken at 1403 K. Nevertheless, the existence of a higher temperature phase seems implausible on chemical grounds as it requires abnormally short Mn-Mn distances and Y–O bonds. From our data we conclude that, in the temperature range 1403 to 1273 K, $YMnO_3$ exists in the $P6_3/mmc$ phase.

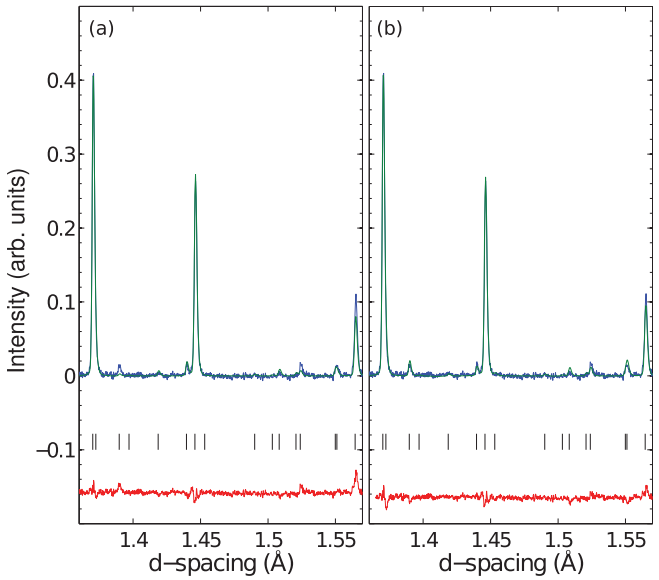

FIG. 5. (Color online) Portions of the Rietveld refinement plots for the 1243-K dataset in (a) $P6_3/mcm$ and (b) $P6_3cm$ models with equal scales. The blue line is the raw data, the green line is the Rietveld fit, and the red line is the difference profile.

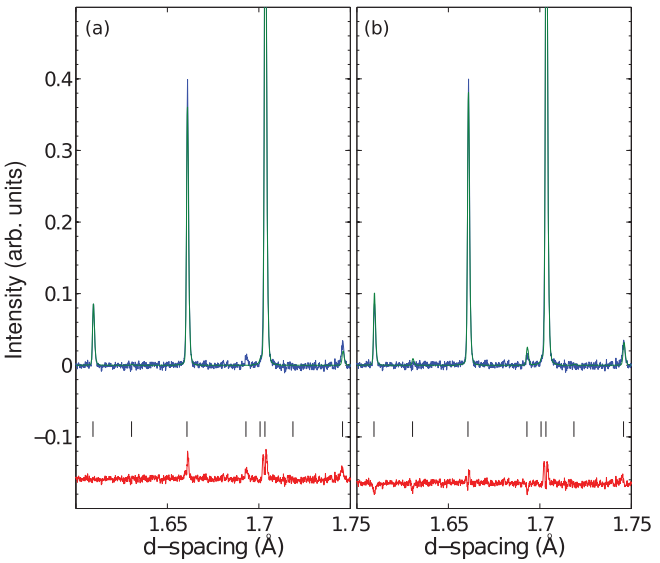

FIG. 6. (Color online) Portions of the Rietveld refinement plots for the 1243-K dataset in (a) $P6_3/mcm$ and (b) $P6_3cm$ models with equal scales. The blue line is the raw data, the green line is the Rietveld fit, and the red line is the difference profile.

B. The unit-cell tripled phases

The dataset immediately below the tripling transition was refined against $P6_3cm$ and $P6_3/mcm$ models to check for the existence of the previously proposed intermediate phase. Both refinements followed the same strategy with the same time-of-flight range, background type, and number of background coefficients. Individual isotropic thermal displacement parameters were refined for all atoms.

Figure 4 shows the plot resulting from the Rietveld refinement in space group $P6_3cm$ and Figs. 5 and 6 show plots of the comparative refinements over selected d-spacing ranges. The $P6_3/mcm$ phase proposed by Nénert et al.[18] and Abrahams[22] gave a poorer refinement judged by both R factors and by eye. The refined structural parameters and the wR_p and χ^2 values for the $P6_3cm$ model are shown in Table III. The parameters for the $P6_3/mcm$ model are included in the supplemental information.[27]

Two specific points may be noted in the $P6_3/mcm$ refinement. First, the refined x parameter of O1 is within error of

TABLE III. The structural parameters for the 1243-K data refined in $P6_3cm$ (No. 185). The lattice parameters are $a = 6.258\,33(4)$ Å and $c = 11.349\,18(12)$ Å (Ref. 26). The refinement gave $wR_p = 0.0284$, $\chi^2 = 4.854$.

Atom	Wyckoff position	x	y	z	$u_{iso} \times 100$ (Å^2)
Y1	2*a*	0	0	0.2639(5)	2.43(11)
Y2	4*b*	$\frac{1}{3}$	$\frac{2}{3}$	0.2399(4)	2.58(7)
Mn	6*c*	0.3094(6)	0	0	1.62(6)
O1	6*c*	0.3297(7)	0	0.1656(4)	2.55(9)
O2	6*c*	0.6621(7)	0	0.3394(4)	2.98(10)
O3	2*a*	0	0	0.5083(7)	3.34(17)
O4	4*b*	$\frac{1}{3}$	$\frac{2}{3}$	0.0153(5)	3.18(10)

TABLE IV. The structural parameters from the Rietveld refinement of the 293-K data in space group $P6_3cm$ (No. 185). The unit-cell parameters are $a = 6.141\,51(9)$ Å and $c = 11.4013(2)$ Å (Ref. 26). The refinement gave $wR_p = 0.0330$ and $\chi^2 = 5.885$.

Atom	Wyckoff position	x	y	z	$u_{iso} \times 100$ (Å^2)
Y1	2*a*	0	0	0.2728(5)	1.16(7)
Y2	4*b*	$\frac{1}{3}$	$\frac{2}{3}$	0.2325(4)	1.30(5)
Mn1	6*c*	0.3177(9)	0	0	0.80(5)
O1	6*c*	0.3074(4)	0	0.1626(4)	1.55(7)
O2	6*c*	0.6427(3)	0	0.3355(4)	1.05(6)
O3	2*a*	0	0	0.4744(6)	1.25(10)
O4	4*b*	$\frac{1}{3}$	$\frac{2}{3}$	0.0169(5)	1.42(7)

$\frac{1}{3}$ (i.e., the allowed displacement does not occur). Second, the thermal displacement parameter u_{iso} for the equatorial oxygen O3 (corresponding to O4 in the $P6_3cm$ model) is almost twice as large as the other two oxygen thermal displacement parameters. Indeed, anisotropic refinement of this atom shows a highly elongated ellipsoid (due to a large u_{33} parameter). This indicates that the continued imposition of the mirror symmetry perpendicular to c in the tripled cell is physically unreasonable and the equatorial oxygen plane is, in reality, tilted. On removal of the mirror plane (i.e., in the polar $P6_3cm$ model), both of the equatorial oxide sites and the yttrium sites are allowed to relax their z coordinates, leading to significant displacements and more reasonable u_{iso} values. The supplemental information[27] contains an additional plot of the raw data and reflection markers for the reflections, which would violate the c-glide reflection conditions of $P6_3cm$ and $P6_3/mcm$. No reflections breaking these conditions were observed, which confirms the restriction of possible space groups to $P6_3cm$ or $P6_3/mcm$.

The Rietveld refinements were performed for all datasets up to the unit-cell tripling transition in space group $P6_3cm$. The data above the transition were refined in $P6_3/mmc$. The refined structural parameters for the room-temperature data

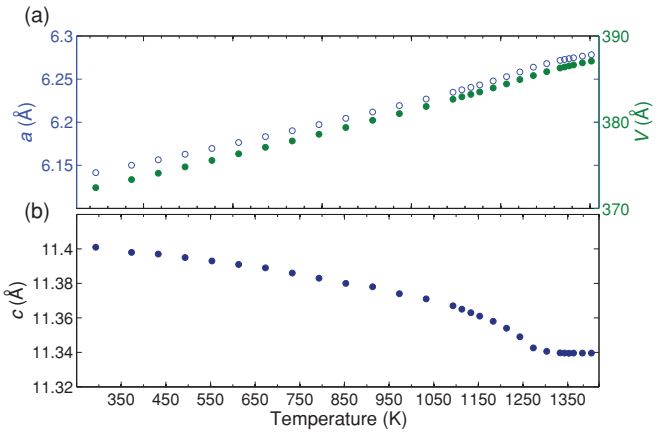

FIG. 7. (Color online) (a) The a-axis parameter (blue open circles) and unit-cell volume (green closed circles) temperature dependences. The a-axis parameters from the high-temperature phase refinements are scaled by $\sqrt{3}$ for clarity. (b) The variation of c-axis parameter with temperature.

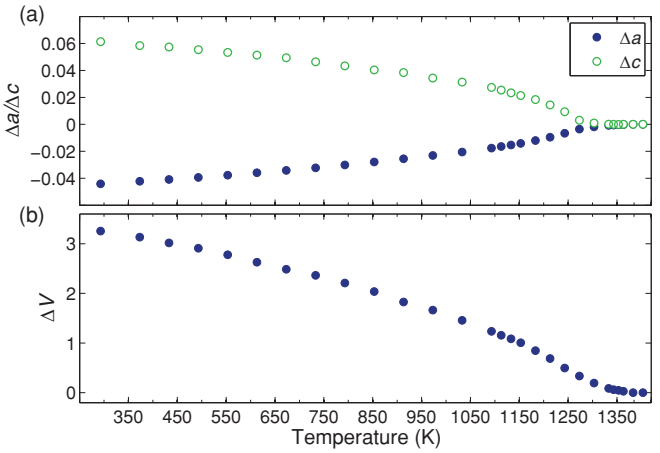

FIG. 8. (Color online) (a) The c-axis lattice parameter (green open circles) and the a-axis parameter (blue closed circles) with a linear temperature dependence (linear fit to highest temperature data) subtracted. (b) The volume of the unit cell with the linear part of the temperature dependence removed.

are shown in Table IV and are in very good agreement with previous single-crystal studies.[11]

Figure 7 shows the lattice parameters and unit-cell volumes extracted from the refinements. An almost linear temperature dependence of the a-axis parameter (the a-axis parameter obtained from the refinements of data in the high-temperature centrosymmetric phase are scaled by a factor of $\sqrt{3}$) is seen up to about 1100 K, where an increase in gradient becomes noticeable. This is followed by a sharp decrease in gradient near 1270 K. The c-axis parameter decreases until about 1270 K, above which it is roughly constant, and the cell volume shows a similar trend to the a-axis parameter. The standard deviations of the lattice parameters are of the order of 1.5×10^{-5} Å for the a-axis and 4×10^{-5} Å for the c-axis.

The trends in a and V are better seen by removing a linear term from the temperature dependence. This was done by subtracting a simple linear fit to the highest temperature data (where the dependence is effectively linear) and scaling all data points by the 1403-K value. The results of this are shown in Fig. 8 and the change in behavior around 1270 K is clear

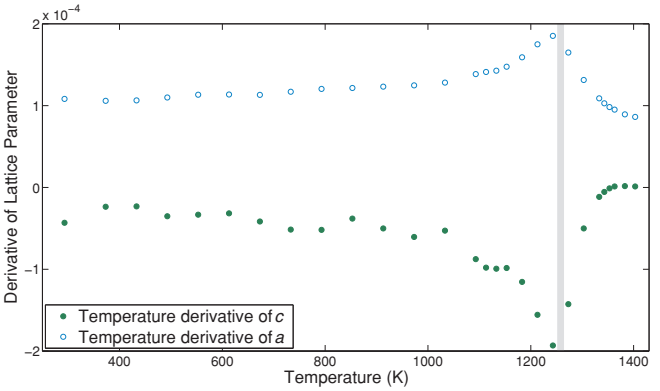

FIG. 9. (Color online) The temperature derivatives of the a (blue open circles) and c (green closed circles) lattice parameters.

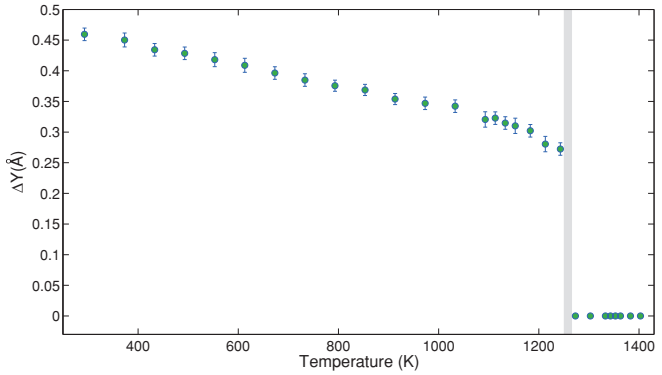

FIG. 10. (Color online) The corrugation of the Y layer, where ΔY is the Y1-Y2 distance in the c direction.

in all three variables. This is confirmed by inspection of the temperature derivatives of a and c shown in Fig. 9.

The tripling of the unit cell directly upon leaving the $P6_3/mmc$ phase removes the possibility of a transition through $P6_3mc$, as this structure would retain the smaller unit cell. From the lattice-parameter derivative data, it is clear that the unit-cell tripling transition is in the range 1258 ± 14 K, which confirms the direct evidence from the superlattice peaks presented in Fig. 3 and in the supplemental information.[27]

The corrugation of the Y^{3+} layers may also be examined to investigate displacements occurring as the system moves toward the high-temperature centrosymmetric phase. This phase has a single Y^{3+} site with $\bar{3}m$ symmetry at fractional coordinates (0,0,0). When the symmetry is lowered, the mirror plane is lost and two of the six Y^{3+} ions displace upward along z (Y1, Wyckoff site 2a), while four displace downward (Y2, Wyckoff site 4b) from the centrosymmetric position. The sum of the c-axis displacements, in Å for a single ion from each site $\Delta Y = \Delta(Y1)_z + \Delta(Y2)_z$, is shown in Fig. 10. The corrugation increases from 0 in the $P6_3/mmc$ phase to about 0.27 Å sharply and then increases smoothly with decreasing temperature.

C. Secondary transition

In the higher symmetry $P6_3/mmc$ phase, the MnO_5 trigonal bipyramids are untilted. It can be seen from Fig. 11 that

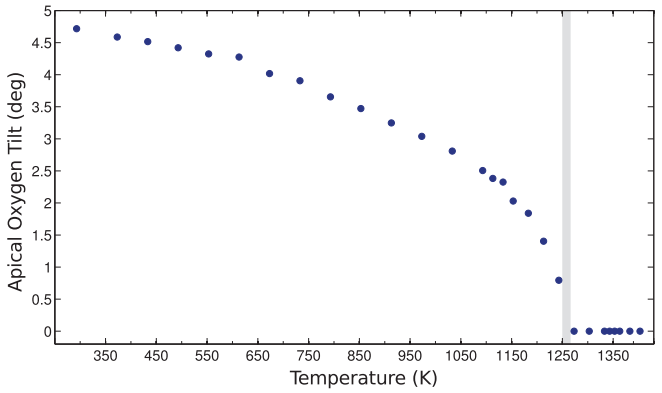

FIG. 11. (Color online) The tilt angle calculated for the Mn apical oxygens (O1 and O2) relative to the c-axis.

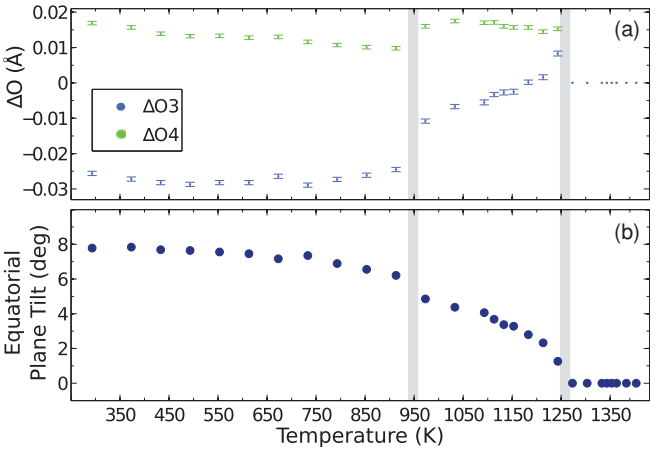

FIG. 12. (Color online) (a) The displacements of O3 (blue) and O4 (green) from their centrosymmetric positions in the z direction. (b) The tilt of the equatorial oxygen plane with respect to the ab plane.

the evolution of apical tilt angle (calculated by taking the angle of O1-O2 to the c-axis direction) with decreasing temperature is relatively smooth, being fixed to zero by symmetry at and above 1273 K. Inspection of the O3 and O4 z coordinates, shown in Fig. 12(a), shows a feature around 913 K with both z coordinates suddenly decreasing. The displacement of O3, in particular, increases markedly with decreasing temperature, moving below the Mn ion for $T \leqslant 853$ K. Figure 12(b) shows the tilt of the equatorial oxygen plane with temperature (angle of O3-O4 to the ab plane), and there is a sharp increase at $T \leqslant 913$ K. The sudden decrease in O3(z) and O4(z) and increase in the equatorial oxygen plane tilt would correspond to a sharp decrease in polarization. This would account for the peak in pyroelectric current seen by Ismailzade and Kizhaev[13] as the pyroelectric current is proportional to $\frac{\partial P}{\partial T}$ for constant heating rate. The resistivity data of Katsufuji *et al.*[15] and Choi *et al.*[2] also show a crossover in resistivity behavior in this temperature region.

The Y–O bond lengths shown in Fig. 13 vary smoothly within error bars except for around 913 K, where there is a

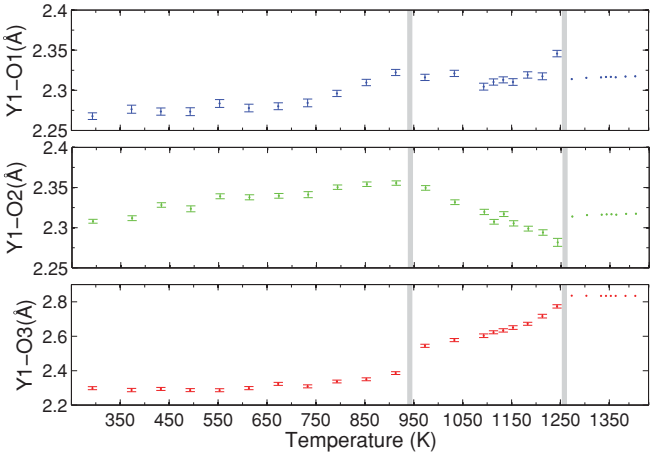

FIG. 13. (Color online) The Y1–O bond lengths determined from the Rietveld refinements.

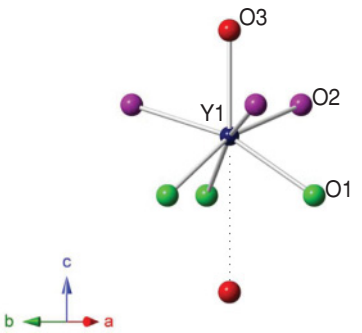

FIG. 14. (Color online) The coordination of the Y1 ion in the low-temperature $P6_3cm$ structure. The bond lengths at room temperature obtained from the Rietveld refinement are Y1-O1 = 2.267(4) Å, Y1-O2 = 2.308(2) Å, and Y1-O3 = 2.298(8) Å. The distance to the other O3 ion (indicated by the dotted line) is 3.402(8) Å.

sudden decrease in the Y1–O3 bond length. This corresponds to the bonding change seen by Kim *et al.*[20] These authors observed hybridization of Y1 and O3 between 910 and 930 K by maximum entropy method (MEM) analysis of the electron density from synchrotron x-ray data. The O3 coordinates the Y1 site apically, whereas the O1 and O2 coordinate it in the equatorial direction, as shown in Fig. 14. The concordance of the structural changes seen in this study with the pyroelectric current, resistivity, and x-ray diffraction data strongly suggest that there is an isosymmetric phase transition (defined by Christy[28] as one in which the space-group symmetry and Wyckoff position occupations are preserved) taking place at $\approx$920 K.

The program AMPLIMODES (Refs. 29 and 30) was used to examine the magnitude of the Γ_1^+, Γ_2^-, K_1, and K_3 distortion modes of $P6_3/mmc$. The results are shown in Fig. 15. The nature of these distortion modes can also be examined and visualized using ISODISPLACE.[31] Γ_1^+ corresponds to a symmetric breathing mode with the order parameter being the change in z coordinate of the apical oxygen O1. Γ_2^- involves a polar displacement of the ions along the c-axis,

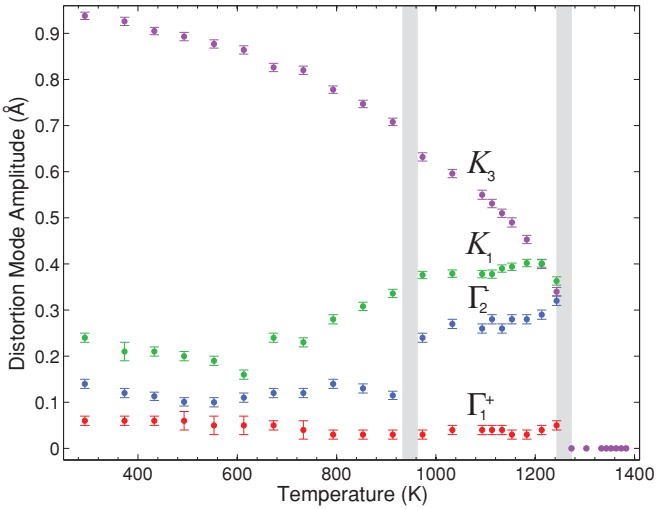

FIG. 15. (Color online) The amplitudes of the distortion modes calculated using AMPLIMODES (Refs. 29 and 30). Above 1243 K, all mode amplitudes are zero and are included for completeness only.

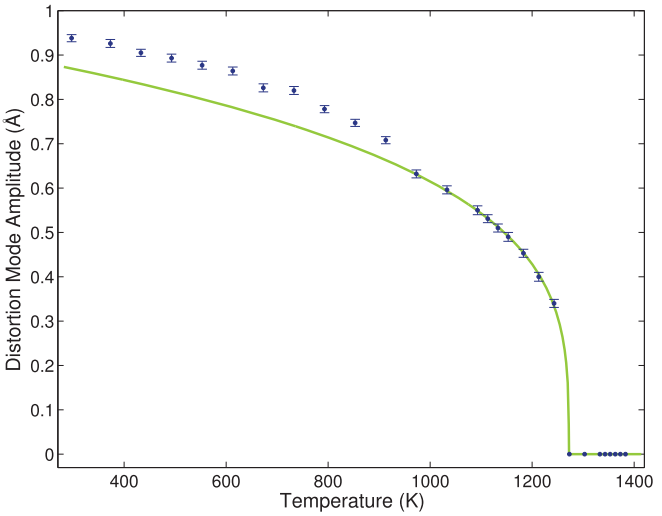

FIG. 16. (Color online) Fit of the K_3 distortion mode amplitude to $K_3 = A(T_C - T)^\beta$.

leading ultimately to the space group $P6_3mc$. K_1 leads to the space group $P6_3/mcm$ by allowing only the O-Mn-O axis to displace in the ab plane, tripling the unit cell. K_3 is the antiferrodistortive mode leading to $P6_3cm$ by a tilt of the MnO_5 bipyramids and antiparallel displacements of the Y^{3+} cations leading to unit-cell tripling. A weighted power-law fit[32] of the form $K_3 = A(T_C - T)^\beta$ was performed on the K_3 data as a function of temperature in the range 913 to 1243 K (the result is shown in Fig. 16). The critical exponent obtained was $\beta = 0.271 \pm 0.003$ with $T_C = 1271.5 \pm 0.1$ K and $A = 0.135 \pm 0.002$. This exponent could be taken to suggest a possible order-disorder–type transition although more data points near the critical temperature would be required for a more reliable characterization. As a check on the reproducibility of our results, the data tabulated by Jeong *et al.*[19] at 1000, 1050, 1100, and 1200 K were used for a

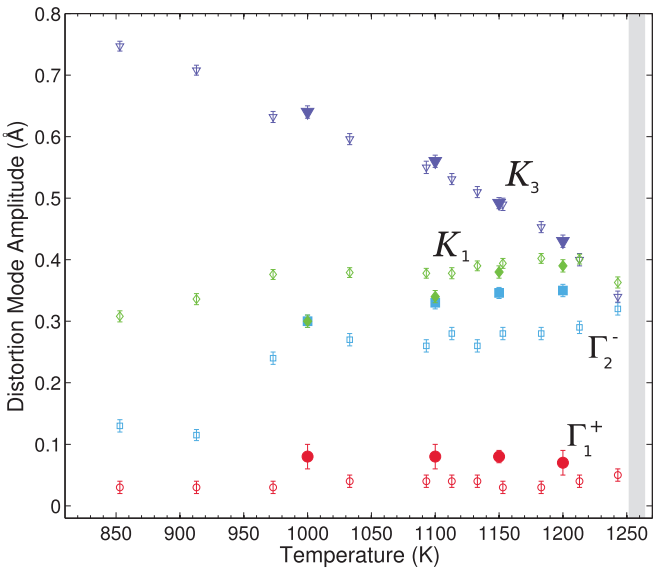

FIG. 17. (Color online) Comparison of the mode amplitudes obtained in this study (open symbols) with those calculated from the data tabulated in Jeong *et al.* (Ref. 19) (larger closed symbols.)

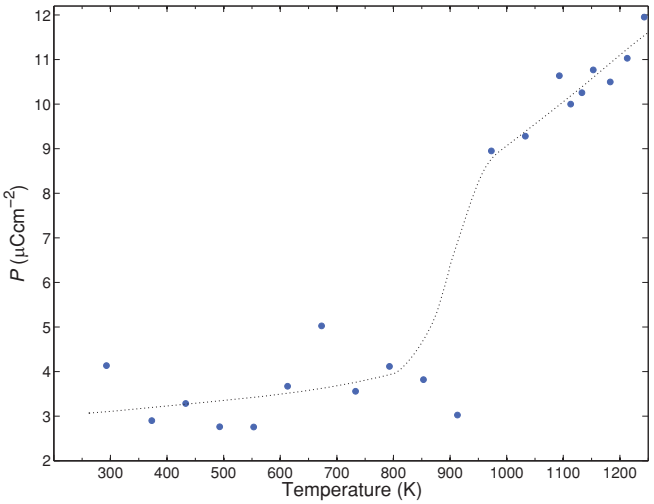

FIG. 18. (Color online) The polarization of $YMnO_3$ estimated using a simple ionic model with the nuclear positions obtained from the Rietveld refinements. The dotted line is a guide to the eye.

similar analysis of the distortion mode amplitudes. As can be seen in Fig. 17, this independently obtained data agree well with our own results within the temperature range studies by Jeong *et al.*

It is clear that the K_3 mode is dominant in general, although the K_1 mode amplitude is slightly larger for the 1243-K dataset [we note that this results almost exclusively from a significant displacement of the Mn x coordinate;[27] since the Mn atom has the smallest neutron scattering length, this is the least well-determined positional parameter in this study]. These dataset was refined in both $P6_3/mcm$ and $P6_3cm$ space groups as already stated, and $P6_3cm$ gave the better fit. At the secondary transition (≈920 K), the amplitude of the Γ_2^- mode decreases abruptly and the K_3 mode shows a small step increase. This would (as a partial contribution to the polarization of the $P6_3cm$ structure) cause a sharp decrease in the polarization and corresponds to the behavior seen in O3 and O4 parameters. The polarization was estimated for the refined structures using a simple ionic model

$$P = \sum_i \frac{\Delta c_i Q_i e m_i}{V},$$

where Δc_i is the displacement of the site from the centrosymmetric position in Å, Q_i is the ionic charge, e is the electron charge, the site multiplicity is denoted by m_i and the unit cell volume is denoted by V. The results of this estimate are shown in Fig. 18.

IV. CONCLUSIONS

In summary, our data confirm that there is no intermediate phase (of the proposed $P6_3/mcm$ symmetry or any other candidate symmetries) between the high-temperature paraelectric $P6_3/mmc$ phase and the unit-cell tripled polar $P6_3cm$ phase. This transition occurs between 1243 and 1273 K and is driven primarily by a nonpolar displacement mode of K_3 symmetry in agreement with earlier theoretical works.[10] Hexagonal $YMnO_3$ is, therefore, an improper ferroelectric, with the antiferrodistortive K_3 mode triggering a weaker, polar distortion of Γ_2^- type. Although there is no clearly defined intermediate phase of differing crystallographic symmetry, our data provide subtle, but compelling, evidence of a secondary isosymmetric transition in the $P6_3cm$ regime at around 920 K. This transition involves polar displacements of the Mn-O equatorial planes, and may be related to an electronic transition involving hybridization of the Y1–O3 bond. After submission of this manuscript, a paper by Kim *et al.*[33] was published involving distortion-mode analysis of synchrotron x-ray data in the range 300 to 1000 K. Their data agree qualitatively with our own, including, significantly, the behavior of the K_3 and Γ_2^- modes at the ≈920-K transition. That the same behavior is seen in two independent studies using different diffraction techniques is an indication that the behavior is indeed intrinsic to the material and reproducible in separately prepared samples. Perhaps surprisingly, this isosymmetric transition leads to a *decreased* polarization but nevertheless does agree with the various anomalies in physical properties reported around this temperature.

ACKNOWLEDGMENT

The authors thank the EPSRC and STFC for funding, K.E. Johnston for experimental assistance, and F.D. Morrison for discussions.

*pl@st-andrews.ac.uk

[1] S. Lee, A. Pirogov, M. S. Kang, K. H. Jang, M. Yonemura, T. Kamiyama, S. W. Cheong, F. Gozzo, N. Shin, H. Kimura, Y. Noda, and J. G. Park, Nature (London) **451**, 805 (2008).

[2] T. Choi, Y. Horibe, H. T. Yi, Y. J. Choi, W. D. Wu, and S. W. Cheong, Nat. Mater. **9**, 253 (2010).

[3] J.-S. Zhou, J. B. Goodenough, J. M. Gallardo Amores, E. Morán, M. A. Alario-Franco, and R. Caudillo, Phys. Rev. B **74**, 014422 (2006).

[4] H. L. Yakel, W. C. Koehler, E. F. Bertaut, and E. F. Forrat, Acta Crystallogr. **16**, 957 (1963).

[5] F. Bertaut, F. Forrat, and P. Fang, C. R. Hebd. Seances Acad. Sci. **256**, 1958 (1963).

[6] P. Coeuré, P. Guinet, J. C. Peuzin, G. Buisson, and E. F. Bertaut, in *Proceedings of the International Meeting on Ferroelectricity Held at Prague, Czechoslovakia June 28–July 1, 1966*, edited by V. Dvorak, A. Fouskova, and P. Glogar (Institute of Physics at the Czechoslovak Academy of Sciences, Prague, 1966), Vol. 1, p. 332.

[7] S. C. Abrahams, Acta Crystallogr., Sect. B: Struct. Sci. **57**, 485 (2001).

[8] E. Bertaut and M. Mercier, Phys. Lett. **5**, 27 (1963).

[9] T. Chatterji, S. Ghosh, A. Singh, L. P. Regnault, and M. Rheinstädter, Phys. Rev. B **76**, 144406 (2007).

[10] C. J. Fennie and K. M. Rabe, Phys. Rev. B **72**, 100103 (2005).

[11] B. B. Van Aken, T. T. M. Palstra, A. Filippetti, and N. A. Spaldin, Nat. Mater. **3**, 164 (2004).

[12]D. I. Khomskii, J. Magn. Magn. Mater. **306**, 1 (2006).
[13]I. G. Ismailzade and S. A. Kizhaev, Fiz. Tverd. Tela **7**, 298 (1965) [Solid State Phys. **7**, 236 (1965)].
[14]K. Łukaszewicz and J. Karut-Kalicińska, Ferroelectrics **7**, 81 (1974).
[15]T. Katsufuji, S. Mori, M. Masaki, Y. Moritomo, N. Yamamoto, and H. Takagi, Phys. Rev. B **64**, 104419 (2001).
[16]T. Katsufuji *et al.*, Phys. Rev. B **66**, 134434 (2002).
[17]G. Nénert, Y. Ren, H. T. Stokes, and T. T. M. Palstra, e-print arXiv:cond-mat/0504546.
[18]G. Nénert, M. Pollet, S. Marinel, G. R. Blake, A. Meetsma, and T. T. M. Palstra, J. Phys. Condens. Matter **19**, 466212 (2007).
[19]I. K. Jeong, N. Hur, and T. Proffen, J. Appl. Crystallogr. **40**, 730 (2007).
[20]J. Kim, K. C. Cho, Y. M. Koo, K. P. Hong, and N. Shin, Appl. Phys. Lett. **95**, 132901 (2009).
[21]T. Lonkai, D. G. Tomuta, U. Amann, J. Ihringer, R. W. A. Hendrikx, D. M. Többens, and J. A. Mydosh, Phys. Rev. B **69**, 134108 (2004).
[22]S. C. Abrahams, Acta Crystallogr., Sect. B: Struct. Sci. **65**, 450 (2009).
[23]R. M. Ibberson, W. I. F. David, and K. S. Knight, Rutherford Appleton Laboratory Report No. RAL-92031, 1992 (unpublished).
[24]R. M. Ibberson, Nucl. Instrum. Methods Phys. Res., Sect. A **600**, 47 (2009).
[25]A. C. Larson and R. B. Von Dreele, Los Alamos National Laboratory Report No. LAUR 86–748, 2000 (unpublished).
[26]This scaling of the lattice parameter uncertainty is in line with W. I. F. David, J. Appl. Crystallogr. **37**, 621 (2004), which suggests appropriate scaling factors for Rietveld-derived estimated standard deviations to bring them in to line with true experimental uncertainties (i.e., those which are not limited solely to errors due to counting statistics). The errors now quoted are also of the order of the change in lattice parameters over 1 K, which is the estimated upper bound to our temperature uncertainty.
[27]See supplemental material at [http://link.aps.org/supplemental/10.1103/PhysRevB.83.094111].
[28]A. G. Christy, Acta Crystallogr., Sect. B: Struct. Sci. **51**, 753 (1995).
[29]D. Orobengoa, C. Capillas, M. I. Aroyo, and J. M. Perez-Mato, J. Appl. Crystallogr. **42**, 820 (2009).
[30]J. M. Perez-Mato, D. Orobengoa, and M. I. Aroyo, Acta Crystallogr., Sect. A: Found. Crystallogr. **66**, 558 (2010).
[31]B. J. Campbell, H. T. Stokes, D. E. Tanner, and D. M. Hatch, J. Appl. Crystallogr. **39**, 607 (2006).
[32]The fit was performed using the MFit 4.2 toolbox by M. Zinkin, D. McMorrow, and D. Tennant, available at [http://www.ill.eu/instruments-support/computing-for-science/cs-software/all-software/matlab-ill/mfit/home]. The errors given in the text are the standard errors from the MFit output.
[33]J. Kim, Y. M. Koo, K.-S. Sohn, and N. Shin, Appl. Phys. Lett. **97**, 092902 (2010).